Relationship Between Two Direct Power Control Methods for PWM Rectifiers Under Unbalanced Network

Yongchang Zhang, *Member, IEEE*, Jihao Gao, and Changqi Qu

***Abstract*—Active power control plays an important role in a pulse width modulation (PWM) rectifier under both balanced and unbalanced network conditions. The prior methods to achieve active power oscillation cancellation (APOC) under unbalanced grid voltages are usually implemented by forcing the grid current to track appropriate current references. They require fine tuning work of a current controller and positive-/negative-sequence extraction of grid voltage/currents and/or converter voltage, which complicates the design of the controller. This paper presents two APOC methods in the frame of direct power control (DPC) for the PWM rectifier and reveals their inherent relationship. In the first method, an appropriate power compensation is added to the original power references without modifying the internal control structure. In the second method, a novel definition of reactive power is employed to replace conventional reactive power, which achieves the aim of APOC automatically. Both methods can be easily integrated with existing DPC schemes with a slight modification. The sequence extraction required in prior methods is eliminated. The inherent relationship between these two methods is investigated, and it is found that they are completely equivalent. The two APOC methods are comparatively studied and implemented in the basic table-based DPC. Simulation and experimental results confirm the theoretical study and the effectiveness of the two methods.**

***Index Terms*—Active power oscillation cancellation (APOC), direct power control (DPC), network unbalance, novel reactive power, pulse width modulation (PWM rectifier).**

I. Introduction

THREE-PHASE pulse width modulation (PWM) rectifiers have been widely used in industry applications owing to their advantages of bidirectional power flow, sinusoidal currents, controllable power factor, and good regulation ability of dc-link voltage [1]–[4]. Generally, the main control strategies of the PWM rectifier are voltage-oriented control (VOC) [5] and direct power control (DPC) [6]–[8] during normal network conditions. In VOC, the input active and reactive powers are regulated indirectly by decomposing the grid currents into active and reactive power components and regulating them separately using linear proportional-integral (PI) controllers [9]. Space-vector modulation is employed in VOC to synthesize the reference rectifier voltage vector. VOC guarantees high dynamics and steady-state performance via internal current control loops. However, the final configuration and performance of the VOC system largely depends on the quality of the applied current control strategy [10]. Another efficient control strategy is DPC, which is similar to the one used in direct torque control [7], [11]–[15]. Different with VOC, the strategy for DPC relies on the instantaneous reactive power theory [16] and is based on the evaluation of the active and reactive instantaneous power error values and the voltage vector position without any internal control loop for the currents. In DPC, there is no PWM modulator block; instead, the desired voltage vector for active and reactive power regulation is directly selected from a predefined switching table. As a result, DPC has a very quick dynamic response with a simple structure.

These control techniques have a good performance with balanced input voltages. However, the grid voltage in actual conditions is often not ideal in a real power system; thus, the PWM rectifier designed under ideal grid conditions could appear in an abnormal operating state such as harmonics in the dc output and odd harmonics in the input currents when the grid voltages are unbalanced [17]. To maintain a constant dc-bus voltage, sinusoidal grid currents, and low fluctuations in the active and/or reactive power, many scholars have carried out studies on PWM rectifiers with distorted input voltages. Because VOC is a mature system, many studies on unbalanced network conditions were first carried out in a VOC frame. The authors in [18] first derived the positive-sequence and negative-sequence current references under the condition of constant active power; however, the control of the negative-sequence current is insufficient. In [19]–[21], dual current control schemes have been used with a VOC strategy. Two controllers are required: one for the positive-sequence component and the other for the negative-sequence component. Although these control methods in the VOC frame have a good steady performance, the main problems are that these methods will result in a slow transient response and rely heavily on the fine tuning work of internal current controllers.

Manuscript received January 28, 2016; revised May 15, 2016; accepted July 19, 2016. Date of publication July 21, 2016; date of current version February 2, 2017. This work was supported in part by the National Natural Science Foundation of China under Grants 51577003 and 51207003, in part by the Beijing Natural Science Foundation under Grant 3162012, and in part by the Beijing Nova Program under Grant xx2013001. Recommended for publication by Associate Editor T. Shimizu.

Y. Zhang is with the Inverter Technologies Engineering Research Center of Beijing, North China University of Technology, Beijing, 100144, China, with the Collaborative Innovation Center of Electric Vehicles in Beijing, and with the Collaborative Innovation Center of Key Power Energy-Saving Technologies in Beijing (e-mail: yozhang@ieee.org).

J. Gao and C. Qu are with the Inverter Technologies Engineering Research Center of Beijing, North China University of Technology, Beijing, 100144, China (e-mail: 275102641@qq.com; qcqdhr@sina.com).

Color versions of one or more of the figures in this paper are available online at http://ieeexplore.ieee.org.

Digital Object Identifier 10.1109/TPEL.2016.2593723

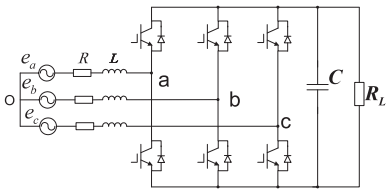

Fig. 1. Topology of a two-level PWM rectifier.

Other studies have been carried out for unbalanced conditions in the DPC frame. The authors in [22] obtained the power compensation by decomposing the positive and negative sequences of both the voltage and current components. However, this can only achieve a single control target that eliminates the negative-sequence current. The authors in [23] achieve different control targets without the extraction of the negative-sequence current components, but the stator and rotor currents contain too many harmonics. The power compensation block was simplified in [24] by eliminating the extraction of the negative-sequence current. Unfortunately, it is still necessary to extract the negative-sequence grid voltages and positive-sequence grid currents to achieve appropriate power compensation.

With the extensive research in PWM rectifiers for unbalanced conditions, a novel definition for the reactive power is proposed that is more suitable than the traditional definition for an unbalanced system [4], [25]–[27]. The authors in [27] use this novel reactive power and obtain good performance; however, the sequential component must also be extracted. The authors in [28] use the novel reactive power and do not require the extraction of any sequence components to obtain a current reference in a stationary frame, but proportional resonance controllers are required to regulate the current. Recently, the novel reactive power has been applied in table-based DPC and achieves APOC automatically with very simple structure [6].

Since APOC can be achieved by various control methods, it is interesting to investigate whether these methods with the same control target have also the same performance, especially for the methods using conventional power theory and novel reactive power definition, which requires a comparative study. Furthermore, the inherent relationship among them should be revealed, which helps to understand the usefulness of the novel reactive power and may stimulate more efficient control methods with lower complexity and higher performance. This is one of the main motivations of this paper.

For simplicity, this paper takes the simple table-based DPC as an example and presents two APOC methods based on table-based DPC. The first APOC method is an improved version of [24] by eliminating the sequence extraction of both grid voltages and currents. As a result, the control complexity is much reduced while achieving the same target. Different from the first method, which uses the conventional reactive power and power compensation technique, the second one uses the novel reactive power without any power compensation technique [6]. Hence, it is much simpler in the structure. In fact, the control structure of the second method is the same as conventional DPC, except that the reactive power is replaced by the new reactive power. Furthermore, the inherent relationship between these two kinds of methods is investigated by studying the underlying mechanism in them using strict mathematical tools. To clearly show the relationship between these two methods, the same switching table is used. The effectiveness of the two methods and their inherent relationship are confirmed by the presented simulation and experimental results.

II. Model of the PWM Rectifier Under Unbalanced Network

The circuit of a three-phase PWM rectifier is shown in Fig. 1. By using the three-phase to two-phase transformation

$$\boldsymbol{x}_{\alpha\beta} = \frac{2}{3}(x_a + \alpha x_b + \alpha^2 x_c) \tag{1}$$

where $x_{a,b,c,}$ is the variable in three-phase frame and $\alpha = e^{j\frac{2}{3}\pi}$, the mathematical model of the PWM rectifier in the two-phase stationary $\alpha\beta$ frame is expressed as [2]

$$\boldsymbol{e}_{\alpha\beta} = R\boldsymbol{i}_{\alpha\beta} + L\frac{d\boldsymbol{i}_{\alpha\beta}}{dt} + \boldsymbol{v}_{\alpha\beta} \tag{2}$$

where $\boldsymbol{v}_{\alpha\beta}$, $\boldsymbol{e}_{\alpha\beta}$, and $\boldsymbol{i}_{\alpha\beta}$ are the rectifier voltage vector, grid voltage vector, and grid current vector, respectively; R and L are the equivalent series resistance and inductance of grid filter, respectively.

The complex power $\boldsymbol{S}$ on the grid side can be calculated from the instantaneous theory as [16]

$$\boldsymbol{S} = \frac{3}{2}\left(\boldsymbol{i}^*_{\alpha\beta}\boldsymbol{e}_{\alpha\beta}\right) = P + jQ \tag{3}$$

where "*" denotes the conjugate of complex vector.

Under unbalanced network conditions, the grid voltages and currents can be expressed as [19]

$$\boldsymbol{e}_{\alpha\beta} = \boldsymbol{e}^+_{dq}e^{j\omega t} + \boldsymbol{e}^-_{dq}e^{-j\omega t} \tag{4}$$

$$\boldsymbol{i}_{\alpha\beta} = \boldsymbol{i}^+_{dq}e^{j\omega t} + \boldsymbol{i}^-_{dq}e^{-j\omega t} \tag{5}$$

where $\boldsymbol{e}^+_{dq} = e^+_d + je^+_q$, $\boldsymbol{e}^-_{dq} = e^-_d + je^-_q$, $\boldsymbol{i}^+_{dq} = i^+_d + ji^+_q$, and $\boldsymbol{i}^-_{dq} = i^-_d + ji^-_q$. Throughout this paper, it is assumed that $\omega = 2\pi f = 314$.

The delayed value of unbalanced grid voltage $\boldsymbol{e}'_{\alpha\beta}$ can be expressed as

$$\begin{aligned}\boldsymbol{e}'_{\alpha\beta} &= \boldsymbol{e}^+_{dq}e^{j(\omega t-\frac{\pi}{2})} + \boldsymbol{e}^-_{dq}e^{-j(\omega t-\frac{\pi}{2})} \\ &= -j\boldsymbol{e}^+_{dq}e^{j\omega t} + j\boldsymbol{e}^-_{dq}e^{-j\omega t} = -j\boldsymbol{e}^+_{\alpha\beta} + j\boldsymbol{e}^-_{\alpha\beta}.\end{aligned} \tag{6}$$

The instantaneous input powers P and Q under unbalanced grid conditions can be expressed as [19]

$$\begin{cases} P &= P_0 + P_{c2}\cos(2\omega t) + P_{s2}\sin(2\omega t) \\ Q &= Q_0 + Q_{c2}\cos(2\omega t) + Q_{s2}\sin(2\omega t) \end{cases} \tag{7}$$

where

$$\begin{cases} P_0 &= \frac{3}{2}(\boldsymbol{i}_{dq}^{+} \odot \boldsymbol{e}_{dq}^{+} + \boldsymbol{i}_{dq}^{-} \odot \boldsymbol{e}_{dq}^{-}) \\ P_{c2} &= \frac{3}{2}(\boldsymbol{i}_{dq}^{-} \odot \boldsymbol{e}_{dq}^{+} + \boldsymbol{i}_{dq}^{+} \odot \boldsymbol{e}_{dq}^{-}) \\ P_{s2} &= \frac{3}{2}(\boldsymbol{i}_{dq}^{+} \otimes \boldsymbol{e}_{dq}^{-} - \boldsymbol{i}_{dq}^{-} \otimes \boldsymbol{e}_{dq}^{+}) \\ Q_0 &= \frac{3}{2}(\boldsymbol{i}_{dq}^{+} \otimes \boldsymbol{e}_{dq}^{+} + \boldsymbol{i}_{dq}^{-} \otimes \boldsymbol{e}_{dq}^{-}) \\ Q_{c2} &= \frac{3}{2}(\boldsymbol{i}_{dq}^{+} \otimes \boldsymbol{e}_{dq}^{-} + \boldsymbol{i}_{dq}^{-} \otimes \boldsymbol{e}_{dq}^{+}) \\ Q_{s2} &= \frac{3}{2}(-\boldsymbol{i}_{dq}^{+} \odot \boldsymbol{e}_{dq}^{-} + \boldsymbol{i}_{dq}^{-} \odot \boldsymbol{e}_{dq}^{+}). \end{cases} \tag{8}$$

III. Principle of APOC

A. Method I

In this paper, the control aim is to obtain sinusoidal grid current and average unity power factor while eliminating the oscillations in the active power. Therefore, the specific control aim can be expressed in the following equations:

$$\begin{cases} P_0 &= \frac{3}{2}(\boldsymbol{i}_{dq}^{+} \odot \boldsymbol{e}_{dq}^{+} + \boldsymbol{i}_{dq}^{-} \odot \boldsymbol{e}_{dq}^{-}) = P^{\text{ref}} \\ Q_0 &= \frac{3}{2}(\boldsymbol{i}_{dq}^{+} \otimes \boldsymbol{e}_{dq}^{+} + \boldsymbol{i}_{dq}^{-} \otimes \boldsymbol{e}_{dq}^{-}) = 0 \\ P_{c2} &= \frac{3}{2}(\boldsymbol{i}_{dq}^{-} \odot \boldsymbol{e}_{dq}^{+} + \boldsymbol{i}_{dq}^{+} \odot \boldsymbol{e}_{dq}^{-}) = 0 \\ P_{s2} &= \frac{3}{2}(\boldsymbol{i}_{dq}^{+} \otimes \boldsymbol{e}_{dq}^{-} - \boldsymbol{i}_{dq}^{-} \otimes \boldsymbol{e}_{dq}^{+}) = 0. \end{cases} \tag{9}$$

To simplify the calculation process, in this paper, both original grid voltage vector $\boldsymbol{e}_{\alpha\beta}$ and its delay value $\boldsymbol{e}_{\alpha\beta}^{'}$ would be used instead of the positive-sequence and negative-sequence grid voltage vector. From (4) and (6), we can obtain the positive-sequence and negative-sequence grid voltage vector in their respective synchronous frame as

$$\begin{bmatrix} \boldsymbol{e}_{dq}^{+} \\ \boldsymbol{e}_{dq}^{-} \end{bmatrix} = \frac{1}{2} \begin{bmatrix} e^{-j\omega t} & je^{-j\omega t} \\ e^{j\omega t} & -je^{j\omega t} \end{bmatrix} \begin{bmatrix} \boldsymbol{e}_{\alpha\beta} \\ \boldsymbol{e}_{\alpha\beta}^{'} \end{bmatrix}. \tag{10}$$

Similarly, the positive-sequence and negative-sequence current vector in their respective synchronous frame can be obtained as

$$\begin{bmatrix} \boldsymbol{i}_{dq}^{+} \\ \boldsymbol{i}_{dq}^{-} \end{bmatrix} = \frac{1}{2} \begin{bmatrix} e^{-j\omega t} & je^{-j\omega t} \\ e^{j\omega t} & -je^{j\omega t} \end{bmatrix} \begin{bmatrix} \boldsymbol{i}_{\alpha\beta} \\ \boldsymbol{i}_{\alpha\beta}^{'} \end{bmatrix} \tag{11}$$

where $\boldsymbol{i}_{\alpha\beta}^{'}$ denotes the quadrature current lagging $\boldsymbol{i}_{\alpha\beta}$ by 90 electrical degrees.

According to (8), (10), and (11), the equations in (9) can be expressed by the grid voltages/currents and their delayed value in stationary frame as

$$\begin{cases} P_0 &= \frac{3}{4}(\boldsymbol{i}_{\alpha\beta} \odot \boldsymbol{e}_{\alpha\beta} + \boldsymbol{i}_{\alpha\beta}^{'} \odot \boldsymbol{e}_{\alpha\beta}^{'}) \\ Q_0 &= \frac{3}{4}(\boldsymbol{i}_{\alpha\beta} \otimes \boldsymbol{e}_{\alpha\beta} + \boldsymbol{i}_{\alpha\beta}^{'} \otimes \boldsymbol{e}_{\alpha\beta}^{'}) \\ P_{c2} &= \frac{3}{4}(k_1 \cos(2\omega t) + k_2 \sin(2\omega t)) \\ P_{s2} &= \frac{3}{4}(-k_2 \cos(2\omega t) + k_1 \sin(2\omega t)) \end{cases} \tag{12}$$

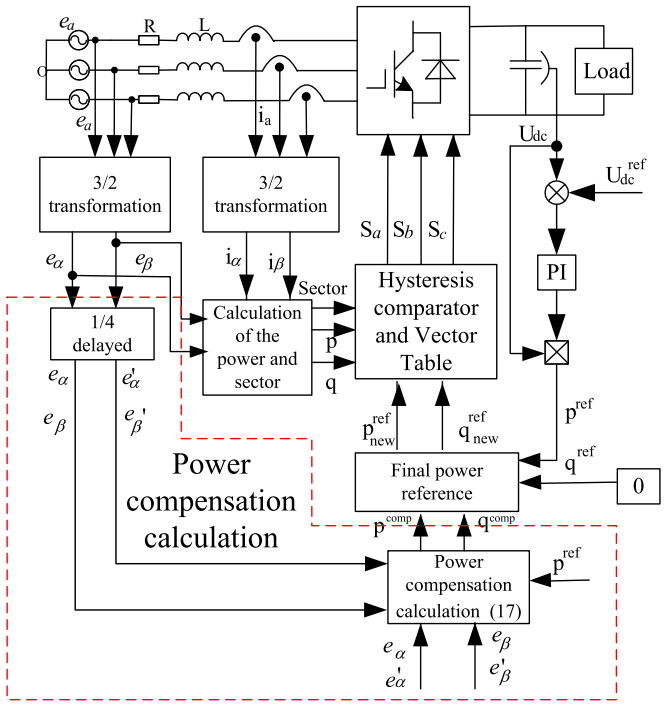

Fig. 2. Control diagram of the APOC method I for the PWM rectifier under unbalanced network conditions.

where

$$\begin{cases} k_1 = & \boldsymbol{i}_{\alpha\beta} \odot \boldsymbol{e}_{\alpha\beta} - \boldsymbol{i}_{\alpha\beta}^{'} \odot \boldsymbol{e}_{\alpha\beta}^{'} \\ k_2 = & \boldsymbol{i}_{\alpha\beta} \odot \boldsymbol{e}_{\alpha\beta}^{'} + \boldsymbol{i}_{\alpha\beta}^{'} \odot \boldsymbol{e}_{\alpha\beta}. \end{cases} \tag{13}$$

Solving (12) is equivalent to solving the following equations:

$$\begin{cases} P_0 &= \frac{3}{4}(\boldsymbol{i}_{\alpha\beta} \odot \boldsymbol{e}_{\alpha\beta} + \boldsymbol{i}_{\alpha\beta}^{'} \odot \boldsymbol{e}_{\alpha\beta}^{'}) = P^{\text{ref}} \\ Q_0 &= \frac{3}{4}(\boldsymbol{i}_{\alpha\beta} \otimes \boldsymbol{e}_{\alpha\beta} + \boldsymbol{i}_{\alpha\beta}^{'} \otimes \boldsymbol{e}_{\alpha\beta}^{'}) = 0 \\ k_1 &= \boldsymbol{i}_{\alpha\beta} \odot \boldsymbol{e}_{\alpha\beta} - \boldsymbol{i}_{\alpha\beta}^{'} \odot \boldsymbol{e}_{\alpha\beta}^{'} = 0 \\ k_2 &= \boldsymbol{i}_{\alpha\beta} \odot \boldsymbol{e}_{\alpha\beta}^{'} + \boldsymbol{i}_{\alpha\beta}^{'} \odot \boldsymbol{e}_{\alpha\beta} = 0. \end{cases} \tag{14}$$

From (14), the final current reference vector is calculated as

$$\boldsymbol{i}_{\alpha\beta}^{\text{ref}} = j\frac{-\frac{2}{3}P^{\text{ref}}\boldsymbol{e}_{\alpha\beta}^{'}}{\boldsymbol{e}_{\alpha\beta} \otimes \boldsymbol{e}_{\alpha\beta}^{'}}. \tag{15}$$

Finally, the new power reference under unbalanced network conditions can be obtained as

$$\boldsymbol{S}_{\text{new}}^{\text{ref}} = \frac{3}{2}\boldsymbol{i}_{\alpha\beta}^{\text{ref}*}\boldsymbol{e}_{\alpha\beta}. \tag{16}$$

Thus, the power compensation is

$$\boldsymbol{S}^{\text{comp}} = \boldsymbol{S}_{\text{new}}^{\text{ref}} - \boldsymbol{S}^{\text{ref}} = j\frac{\boldsymbol{e}_{\alpha\beta} \odot \boldsymbol{e}_{\alpha\beta}^{'}}{\boldsymbol{e}_{\alpha\beta} \otimes \boldsymbol{e}_{\alpha\beta}^{'}}P^{\text{ref}} \tag{17}$$

where $\boldsymbol{S}^{\text{ref}}$ is the traditional power reference. Generally, the reactive power reference is zero to maintain a unity power factor.

The control diagram of the method I is illustrated in Fig. 2, where the power compensation calculation (in the dashed block) is implemented in the outer loop and can be easily integrated into

TABLE I
SWITCHING TABLE IN DPC UNDER UNBALANCED NETWORK CONDITION

dP	dQ	select vector
↑	↑	$V_{0,7}$
↑	↓	V_{k-1}
↓	↑	V_{k+1}
↓	↓	V_k

conventional DPC. The power compensation is much simpler than that introduced in [24] by using $\boldsymbol{e}_{\alpha\beta}$ and $\boldsymbol{e}'_{\alpha\beta}$ only. On the contrary, both negative-sequence grid voltages and positive-sequence grid currents are required when calculating the power compensation in [24]. The switching table in Fig. 2 is shown in Table I, where k is the sector number and it is cycling counted. This table is reported to have better steady-state performance than other kinds of switching tables [29].

B. Method II

The principle of method II has been well introduced in [6] and it is briefly revisited in this paper. The novel definition of the reactive power is expressed as [25], [27]

$$Q^{\text{nov}} = \frac{3}{2}\text{Re}\left(\boldsymbol{i}^*_{\alpha\beta}\boldsymbol{e}'_{\alpha\beta}\right) \tag{18}$$

where $\boldsymbol{e}'_{\alpha\beta}$ denotes the variable that lags $\boldsymbol{e}_{\alpha\beta}$ by 90 electrical degrees.

The differentiation of grid voltage $\boldsymbol{e}_{\alpha\beta}$ and its delayed value $\boldsymbol{e}'_{\alpha\beta}$ can be obtained from (4) and (6) as

$$\frac{d\boldsymbol{e}_{\alpha\beta}}{dt} = j\omega\boldsymbol{e}^+_{\alpha\beta} - j\omega\boldsymbol{e}^-_{\alpha\beta} = -\omega\boldsymbol{e}'_{\alpha\beta} \tag{19}$$

$$\frac{d\boldsymbol{e}'_{\alpha\beta}}{dt} = \omega\boldsymbol{e}^+_{\alpha\beta} + \omega\boldsymbol{e}^-_{\alpha\beta} = \omega\boldsymbol{e}_{\alpha\beta}. \tag{20}$$

The differentiation of grid current can be obtained from (2) as

$$\frac{d\boldsymbol{i}_{\alpha\beta}}{dt} = \frac{1}{L}\left(\boldsymbol{e}_{\alpha\beta} - \boldsymbol{v}_{\alpha\beta} - R\boldsymbol{i}_{\alpha\beta}\right). \tag{21}$$

According to (3), (19), and (21), the derivative of active power can be obtained as

$$\frac{dP}{dt} = \frac{3}{2L}\left[\left|\boldsymbol{e}_{\alpha\beta}\right|^2 - \text{Re}\left(\boldsymbol{v}^*_{\alpha\beta}\boldsymbol{e}_{\alpha\beta}\right)\right] - \frac{R}{L}P - \omega Q^{\text{nov}}. \tag{22}$$

Similarly, the differentiation of the novel reactive power can be obtained from (18), (20), and (21) as

$$\frac{dQ^{\text{nov}}}{dt} = \frac{3}{2L}\text{Re}\left[\left(\boldsymbol{e}^*_{\alpha\beta} - \boldsymbol{v}^*_{\alpha\beta}\right)\boldsymbol{e}'_{\alpha\beta}\right] - \frac{R}{L}Q^{\text{nov}} + \omega P. \tag{23}$$

The instantaneous active and reactive powers can be controlled by selecting the proper rectifier voltage vector. Therefore, it is necessary to investigate the influence of each rectifier voltage vector on both the instantaneous active and reactive powers. In the following analysis, the influences of various voltage vectors in all sectors are plotted to obtain the appropriate switching table for simultaneous control of both active and reactive powers during network unbalance.

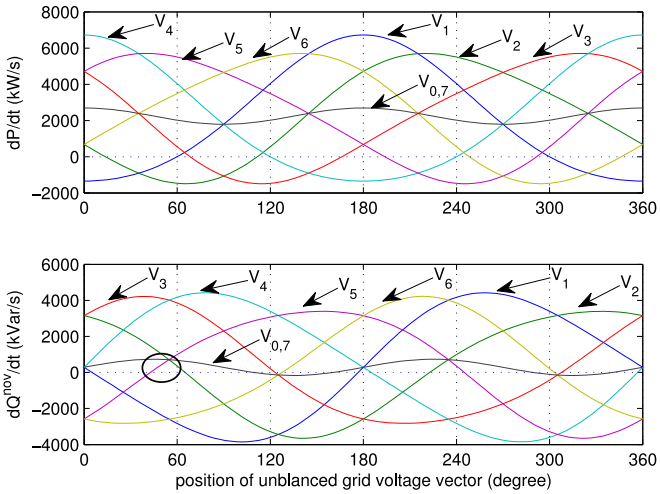

Fig. 3. Slopes of the active/reactive power for various rectifier voltage vectors under unbalanced network conditions using the novel reactive definition (assuming $P = 900$ W and $Q = 0$ Var).

TABLE II.
VECTOR SELECTION TABLE FOR DPC UNDER UNBALANCED NETWORK

dP	dQ	select vectors
↑	↑	$V_0, V_7, V_{k+2}, V_{k+3}$
↑	↓	V_{k-1}, V_{k-2}
↓	↑	V_{k+1}
↓	↓	V_k

According to (22) and (23), the slopes of the active power and the new reactive power versus the grid voltage position for various converter voltage vectors can be calculated. The converter voltage vectors can be expressed as $\boldsymbol{v} = 0$ for zero vectors and $\boldsymbol{v} = \frac{2}{3}U_{dc}e^{j\frac{\pi}{3}(n-1)}$ $(n = 1, 2, ..., 6)$ for nonzero vectors, where U_{dc} is the dc-link voltage. By substituting the converter voltage vector into (22) and (23), the power slopes for various converter voltage vectors can be obtained and are illustrated in Fig. 3. The parameters used to calculate the power slopes of (22) and (23) are: $P = 900$ W, $Q^{\text{nov}} = 0$ Var, $R = 0.3\ \Omega$, $L = 10$ mH, $\omega = 2\pi \times 50 = 314$ rad/s, and $U_{\text{dc}} = 300$ V. The amplitude of positive-sequence voltage vector is $|\boldsymbol{e}^+| = 150 \times \sqrt{2/3} = 122$ V and the amplitude of the negative-sequence voltage vector is assumed to be 10% of positive-sequence voltage vector, i.e., $|\boldsymbol{e}^-| = 0.1\,|\boldsymbol{e}^+|$. Considering that a typical steady-state voltage imbalance is no more than 3% in grid [30], the assumption of a 10% voltage imbalance in this paper is more rigorous. The initial phase angles of the positive and negative-sequence voltage vectors are $\varphi_1 = 0$ and $\varphi_2 = \frac{\pi}{6}$, respectively.

Suppose that the grid voltage vector $\boldsymbol{e}$ is located in the first sector (0–60°). It can be observed from Fig. 3 that there are three vectors increasing both P and Q^{nov} ($\boldsymbol{V}_{0,7}$, $\boldsymbol{V}_3$, and $\boldsymbol{V}_4$) and two vectors ($\boldsymbol{V}_5$ and $\boldsymbol{V}_6$) increasing P and decreasing Q^{nov}, but only one vector when decreasing P ($\boldsymbol{V}_2$ for increasing Q^{nov} and $\boldsymbol{V}_1$ for decreasing Q^{nov}). The influence of the converter voltage vectors on power slopes in other sectors can be analyzed in a similar way. By summarizing the results in Fig. 3, the switching table presented in Table II can be constructed to

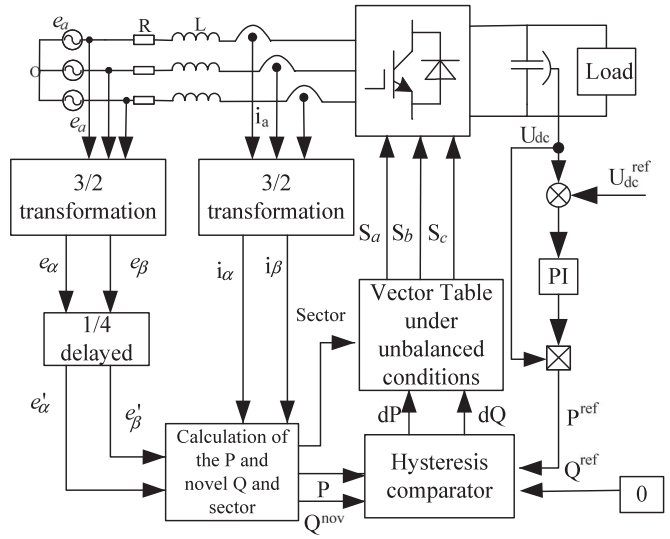

Fig. 4. Control diagram of the APOC method II for PWM rectifier under unbalanced network conditions.

suitably achieves simultaneous control of both P and Q^{nov}. In this paper, the same switching table as Table I out of the several possible switching tables in Table II is employed, and the control diagram of the novel DPC is illustrated in Fig. 4. We can see that method II has the same structure as conventional DPC except that the reactive power is expressed in the form of (18).

C. Relationship Between the Two Methods

In this section, the inherent relationship between the two methods is investigated. In a similar way to (7), the novel reactive power Q^{nov} under unbalanced network can be expressed as

$$\begin{aligned} Q^{\text{nov}} &= \frac{3}{2}\text{Re}\left(\boldsymbol{i}^{*}\boldsymbol{e}^{'}\right) \\ &= \frac{3}{2}\left[\left(\boldsymbol{i}_{dq}^{+}e^{j\omega t}+\boldsymbol{i}_{dq}^{-}e^{-j\omega t}\right)^{*}\left(-j\boldsymbol{e}_{dq}^{+}e^{j\omega t}+j\boldsymbol{e}_{dq}^{-}e^{-j\omega t}\right)\right] \\ &= Q_0^{\text{nov}}+Q_{c2}^{\text{nov}}\cos(2\omega t)+Q_{s2}^{\text{nov}}\sin(2\omega t) \end{aligned} \tag{24}$$

where

$$\begin{cases} Q_0^{\text{nov}} &= \dfrac{3}{2}(\boldsymbol{i}_{dq}^{+}\otimes\boldsymbol{e}_{dq}^{+}-\boldsymbol{i}_{dq}^{-}\otimes\boldsymbol{e}_{dq}^{-}) \\ Q_{c2}^{\text{nov}} &= \dfrac{3}{2}(-\boldsymbol{i}_{dq}^{+}\otimes\boldsymbol{e}_{dq}^{-}+\boldsymbol{i}_{dq}^{-}\otimes\boldsymbol{e}_{dq}^{+}) \\ Q_{s2}^{\text{nov}} &= \dfrac{3}{2}(\boldsymbol{i}_{dq}^{+}\odot\boldsymbol{e}_{dq}^{-}+\boldsymbol{i}_{dq}^{-}\odot\boldsymbol{e}_{dq}^{+}). \end{cases} \tag{25}$$

Substituting (10) and (11) into (25), the gains are now expressed by the variables in the stationary frame and their delayed values as

$$\begin{cases} Q_0^{\text{nov}} &= \dfrac{3}{4}(\boldsymbol{i}_{\alpha\beta}\odot\boldsymbol{e}_{\alpha\beta}^{'}-\boldsymbol{i}_{\alpha\beta}^{'}\odot\boldsymbol{e}_{\alpha\beta}) \\ Q_{c2}^{\text{nov}} &= \dfrac{3}{4}(k_2\cos(2\omega t)-k_1\sin(2\omega t)) \\ Q_{s2}^{\text{nov}} &= \dfrac{3}{4}(k_1\cos(2\omega t)+k_2\sin(2\omega t)) \end{cases} \tag{26}$$

where

$$\begin{cases} k_1 = & \boldsymbol{i}_{\alpha\beta}\odot\boldsymbol{e}_{\alpha\beta}-\boldsymbol{i}_{\alpha\beta}^{'}\odot\boldsymbol{e}_{\alpha\beta}^{'} \\ k_2 = & \boldsymbol{i}_{\alpha\beta}\odot\boldsymbol{e}_{\alpha\beta}^{'}+\boldsymbol{i}_{\alpha\beta}^{'}\odot\boldsymbol{e}_{\alpha\beta}. \end{cases} \tag{27}$$

In method II, the control aim is to track the reference value of active power P^{ref} and novel reactive power $Q^{\text{nov,ref}}$, which can be expressed by the following equations:

$$\begin{cases} P_0 &= \dfrac{3}{4}(\boldsymbol{i}_{\alpha\beta}\odot\boldsymbol{e}_{\alpha\beta}+\boldsymbol{i}_{\alpha\beta}^{'}\odot\boldsymbol{e}_{\alpha\beta}^{'}) = P^{\text{ref}} \\ Q_0^{\text{nov}} &= \dfrac{3}{4}(\boldsymbol{i}_{\alpha\beta}\odot\boldsymbol{e}_{\alpha\beta}^{'}-\boldsymbol{i}_{\alpha\beta}^{'}\odot\boldsymbol{e}_{\alpha\beta}) = 0 \\ P_{c2} &= \dfrac{3}{4}(k_1\cos(2\omega t)+k_2\sin(2\omega t)) = 0 \\ P_{s2} &= \dfrac{3}{4}(-k_2\cos(2\omega t)+k_1\sin(2\omega t)) = 0 \\ Q_{c2}^{\text{nov}} &= \dfrac{3}{4}(k_2\cos(2\omega t)-k_1\sin(2\omega t)) = 0 \\ Q_{s2}^{\text{nov}} &= \dfrac{3}{4}(k_1\cos(2\omega t)+k_2\sin(2\omega t)) = 0. \end{cases} \tag{28}$$

Solving (28) is equivalent to solving the following equations:

$$\begin{cases} P_0 &= \dfrac{3}{4}(\boldsymbol{i}_{\alpha\beta}\odot\boldsymbol{e}_{\alpha\beta}+\boldsymbol{i}_{\alpha\beta}^{'}\odot\boldsymbol{e}_{\alpha\beta}^{'}) = P^{\text{ref}} \\ Q_0^{\text{nov}} &= \dfrac{3}{4}(\boldsymbol{i}_{\alpha\beta}\odot\boldsymbol{e}_{\alpha\beta}^{'}-\boldsymbol{i}_{\alpha\beta}^{'}\odot\boldsymbol{e}_{\alpha\beta}) = 0 \\ k_1 &= \boldsymbol{i}_{\alpha\beta}\odot\boldsymbol{e}_{\alpha\beta}-\boldsymbol{i}_{\alpha\beta}^{'}\odot\boldsymbol{e}_{\alpha\beta}^{'} = 0 \\ k_2 &= \boldsymbol{i}_{\alpha\beta}\odot\boldsymbol{e}_{\alpha\beta}^{'}+\boldsymbol{i}_{\alpha\beta}^{'}\odot\boldsymbol{e}_{\alpha\beta} = 0. \end{cases} \tag{29}$$

After further calculation, the current references satisfying (29) can be obtained as

$$\boldsymbol{i}_{\alpha\beta,\text{nov}}^{\text{ref}} = j\frac{-\frac{2}{3}P^{\text{ref}}\boldsymbol{e}_{\alpha\beta}^{'}}{\boldsymbol{e}_{\alpha\beta}\otimes\boldsymbol{e}_{\alpha\beta}^{'}} \tag{30}$$

which is exactly the same as the current reference in (15) of method I. This means that method II is equivalent to method I, because they have the same current reference in essence.

The corresponding new power references satisfying (29) under unbalanced grid voltage conditions are

$$\begin{aligned} P_{\text{nov}}^{\text{ref}} &= \frac{3}{2}(\boldsymbol{i}_{\alpha\beta,\text{nov}}^{\text{ref}}\odot\boldsymbol{e}_{\alpha\beta}) \\ &= -\frac{P^{\text{ref}}}{\boldsymbol{e}_{\alpha\beta}\otimes\boldsymbol{e}_{\alpha\beta}^{'}}(\boldsymbol{e}_{\alpha\beta}^{'}\otimes\boldsymbol{e}_{\alpha\beta}) = P^{\text{ref}} \end{aligned} \tag{31}$$

$$\begin{aligned} Q_{\text{nov}}^{\text{ref}} &= \frac{3}{2}(\boldsymbol{i}_{\alpha\beta,\text{nov}}^{\text{ref}}\odot\boldsymbol{e}_{\alpha\beta}^{'}) \\ &= -\frac{P^{\text{ref}}}{\boldsymbol{e}_{\alpha\beta}\otimes\boldsymbol{e}_{\alpha\beta}^{'}}(\boldsymbol{e}_{\alpha\beta}^{'}\otimes\boldsymbol{e}_{\alpha\beta}^{'}) = 0 \end{aligned} \tag{32}$$

which are exactly the same as the original power reference in conventional DPC. This means that by using the novel reactive power in method II, it is not necessary to modify the power references by adding a power compensation block, as shown in method I. Hence, method II is much simpler in principle and easier to implement.

The inherent equivalence between the two methods can be further explained as follows. In DPC, the voltage vector is selected according to the value of dP, dQ, and the sector. The two

TABLE III
SYSTEM AND CONTROL PARAMETERS

system	parameters
AC line voltage	150 V
Line resistance	0.3 Ω
Load resistance	97 Ω
Frequency	50 Hz
AC-side inductance	10 mH
DC-bus capacitors	840 μF
DC-bus voltage	300 V
Sampling Frequency	20 kHz

methods use the same vector table; thus, in the same sector, the voltage vector selection is only dependent on the signs of dP and dQ, where

$$\begin{cases} dP &= P^{\text{ref}} - P \\ dQ &= Q^{\text{ref}} - Q. \end{cases} \tag{33}$$

In method I, we have

$$\begin{cases} dP^I &= P^{\text{ref}} + 0 - P \\ dQ^I &= 0 + Q^{\text{comp}} - Q. \end{cases} \tag{34}$$

In method II, we have

$$\begin{cases} dP^{II} &= P^{\text{ref}} - P \\ dQ^{II} &= 0 - Q^{\text{nov}}. \end{cases} \tag{35}$$

From (34) and (35), it is easily observed that $dP^I = dP^{II}$. For the reactive power change, by substituting (3) and (17) into (34) and replacing P^{ref} with its actual value P, we can obtain that

$$\begin{aligned} dQ^I &= \frac{\boldsymbol{e}_{\alpha\beta} \odot \boldsymbol{e}'_{\alpha\beta}}{\boldsymbol{e}_{\alpha\beta} \otimes \boldsymbol{e}'_{\alpha\beta}} P - Q \\ &= \frac{\boldsymbol{e}_{\alpha\beta} \odot \boldsymbol{e}'_{\alpha\beta}}{\boldsymbol{e}_{\alpha\beta} \otimes \boldsymbol{e}'_{\alpha\beta}} \cdot \frac{3}{2} \left(\boldsymbol{i}_{\alpha\beta} \odot \boldsymbol{e}_{\alpha\beta}\right) - \frac{3}{2} \left(\boldsymbol{i}_{\alpha\beta} \otimes \boldsymbol{e}_{\alpha\beta}\right) \\ &= k \cdot \frac{3}{2} \left(\boldsymbol{i}_{\alpha\beta} \odot \boldsymbol{e}'_{\alpha\beta}\right) = k \cdot Q^{\text{nov}} \end{aligned} \tag{36}$$

where $k = |\boldsymbol{e}_{\alpha\beta}|^2 / \left(\boldsymbol{e}_{\alpha\beta} \otimes \boldsymbol{e}'_{\alpha\beta}\right) = 1/\sin\theta$ $(-\pi < \theta < 0)$ is negative and θ is the angle between $\boldsymbol{e}'_{\alpha\beta}$ and $\boldsymbol{e}_{\alpha\beta}$. According to (35) and (36), it is clear that dQ^I and dQ^{II} have the same signs.

In summary, the signs of dP and dQ in methods I and II are exactly the same. Hence, they should select the same voltage vector in the same sector by using the same switching table. Therefore, it can be concluded that method II using the novel reactive power definition is equivalent to the method I using the power compensation technique. This will be further confirmed by the following simulation and experimental results.

IV. SIMULATION RESULTS

To confirm the effectiveness of the two APOC methods and their inherent relationship, simulations have been carried out in MATLAB/Simulink. The system and control parameters are listed in Table III. Fig. 5 shows the simulation results for both methods when the grid voltages become unbalanced at

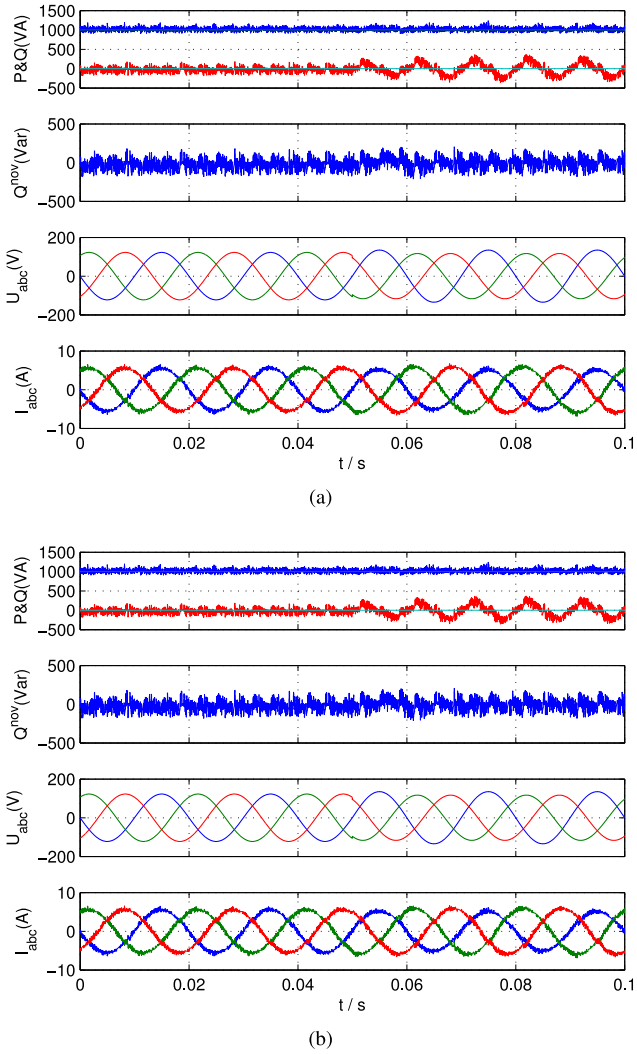

Fig. 5. Simulated steady-state responses when the grid voltages change from the ideal conditions to the unbalanced conditions. (a) Method I. (b) Method II.

$t = 0.05$ s. The curves from top to bottom are as follows: active power, traditional reactive power, novel reactive power, three-phase grid voltages, and three-phase grid currents. From Fig. 5, it is clear that the two methods have a similar performance. Furthermore, the total harmonic distortion (THD) of the grid current of the two methods is 6.38%.

To further demonstrate the equivalence of the two methods, a simulation of the vector selection under the same condition as Fig. 5 is carried out for the two methods, as shown in Fig. 6. Here, again, the grid voltage is disturbed at $t = 0.05$ s. The curves from top to bottom are as follows: the differences between the vector of two methods, vector selection of methods I and II. From Fig. 6, it is clear that the two methods select the same vector at all times, which is in accordance to the theoretical study in Section III-C.

V. EXPERIMENTAL TESTS

Apart from the simulation study, experimental tests have also been carried out to validate the effectiveness of the two APOC methods and their inherent relationship. The experimental setup

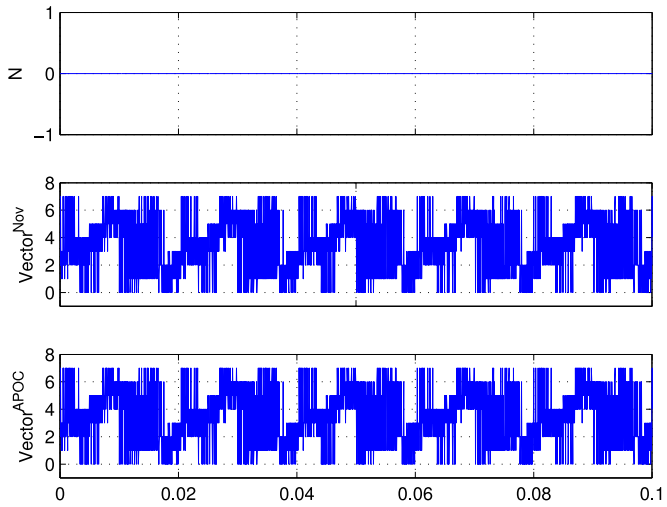

Fig. 6. Simulated vector selection for the two methods.

is the same as that in [6]. For the aim of comparison, the results obtained from conventional DPC using Table I are also presented under ideal and unbalanced grid voltage conditions. These methods are implemented on a 32-bit floating DSP (TMS320F28335) and the sampling period is 50 μs. The system and control parameters are the same as those listed in Table III.

A. Steady-State Performance

First, the experimental tests for the conventional DPC, APOC method I, and APOC method II are presented in Fig. 7, where the grid voltages are first sinusoidal and balanced and then become unbalanced due to one-phase dip. The active power reference is 1000 W, and the reactive power reference is 0 Var to achieve a unity power factor operation. From top to bottom, the curves in Fig. 7 are the active power, traditional reactive power, one-phase grid voltage, and one-phase grid current. It is clearly observed that, under ideal grid voltage conditions, both APOC method I and method II have very similar steady-state performance to conventional DPC, where the grid current is sinusoidal and constant active power and reactive power are achieved. This proves that the APOC methods work well under ideal grid voltage conditions.

However, when the grid voltage become unbalanced, the grid current of conventional DPC is highly distorted. On the contrary, both the APOC method I and method II still present constant active power and maintain sinusoidal grid current, except that the reactive power is now oscillating at twice grid frequency. The results of the both methods are very similar to each other.

Fig. 8 further presents the experimental results obtained under the same condition as Fig. 7, except that the second channel is now the novel reactive power. It is clearly seen that, in method II, constant active power and novel reactive power are achieved while obtaining sinusoidal grid current, even if the grid voltages are unbalanced. In other words, method II can work effectively under both ideal and unbalanced grid voltage conditions without modifying the control structure. Method I can achieve the same targets, however, with the help of power compensation

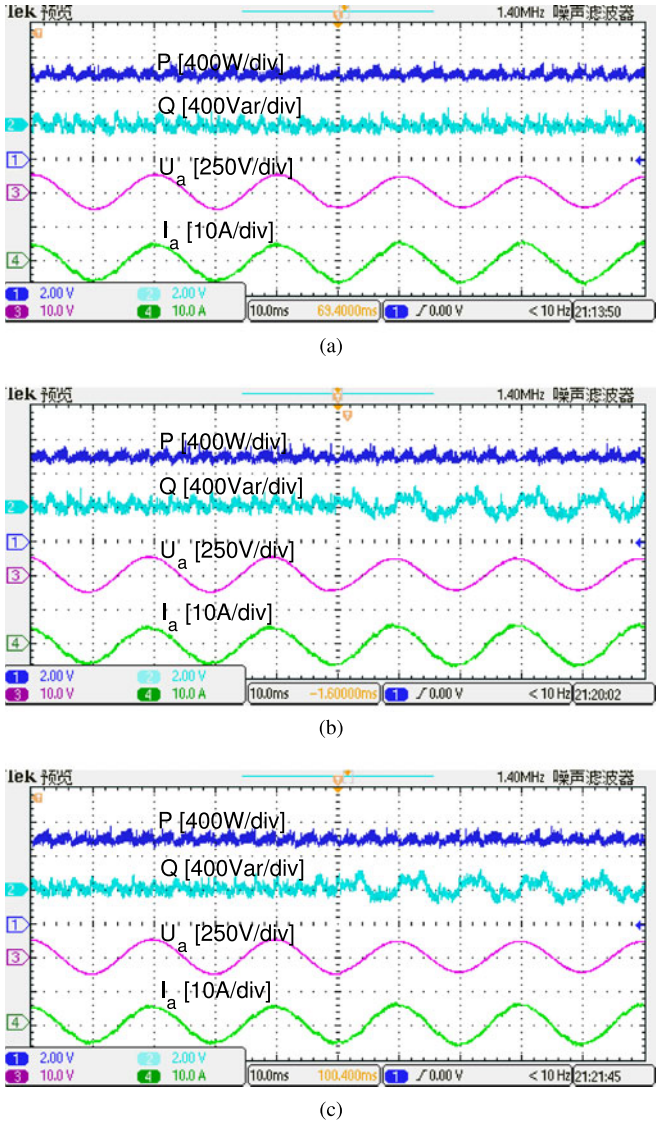

Fig. 7. Experimental waveform of active power, conventional reactive power, one-phase grid voltage, and one-phase grid current when the grid voltages change from the ideal conditions to the unbalanced conditions. (a) Conventional DPC. (b) APOC method I. (c) APOC method II.

technique. It should be noted that in conventional DPC, the novel reactive power is now oscillating at twice grid frequency. The results are in accordance to the simulation results in Fig. 5, validating the theoretical study in Section III.

Under unbalanced grid voltage conditions, the distorted grid current can be improved immediately when the power compensation is added to the original power reference or the feedback reactive power is replaced by the novel reactive power, as shown in Fig. 9. The results obtained under the same testing condition as Fig. 9 are illustrated in Fig. 10, where the second curve is the novel reactive power rather than the conventional reactive power in Fig. 9. It is clear that the two methods can both achieve constant active power and novel reactive power while reducing the current harmonics, irrespective of the grid voltage condition.

Fig. 11 further presents the harmonic spectrum of the grid current at $P = 1000$ W and $Q = 0$ Var for the conventional DPC

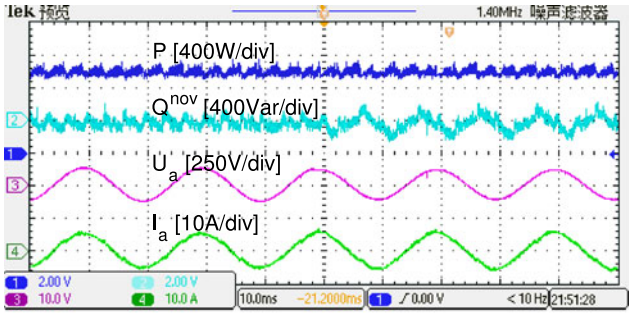

(a)

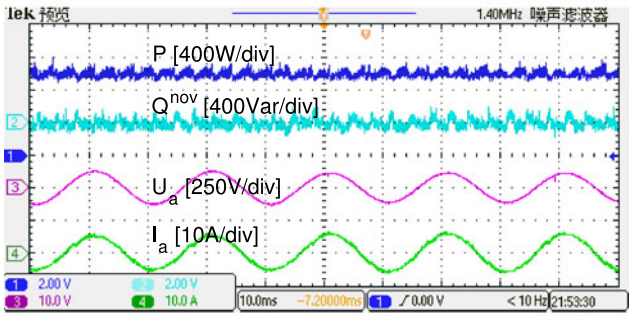

(b)

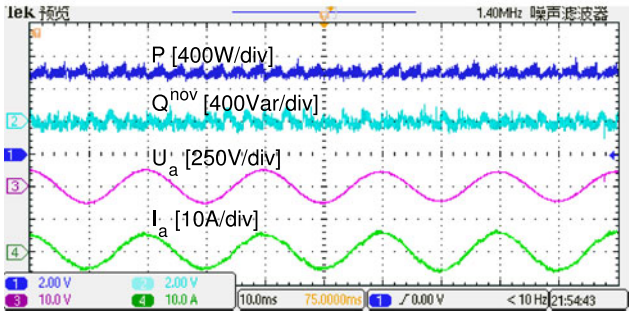

(c)

Fig. 8. Experimental waveform of active power, novel reactive power, one-phase grid voltage, and one-phase grid current when the grid voltages change from the ideal conditions to the unbalanced conditions. (a) Conventional DPC. (b) APOC method I. (c) APOC method II.

and APOC methods I and II. It can be observed that, when the grid voltages are unbalanced, the current harmonic distortion is as high as 8.56% in conventional DPC, which is mainly caused by the low-order harmonics, especially the third harmonics. On the contrary, the current is still sinusoidal in both APOC methods under unbalanced network and they present much lower current THD of 4.70% and 4.74%, which are similar to each other. In fact, in both APOC methods, the grid current is assumed to be sinusoidal, because only positives-sequence and negative-sequence current are allowed to exist when deriving the principle in Section III. Hence, both APOC methods should obtain sinusoidal (and unbalanced) grid currents to achieve constant active power under unbalanced network. However, in practical tests, due to the accuracy of AD sensor, influence of deadtime, and other unmodeled factors, the current harmonics cannot be totally eliminated. Nevertheless, the results prove that the proposed APOC methods are effective in reducing current harmonics while eliminating the oscillation in the active power.

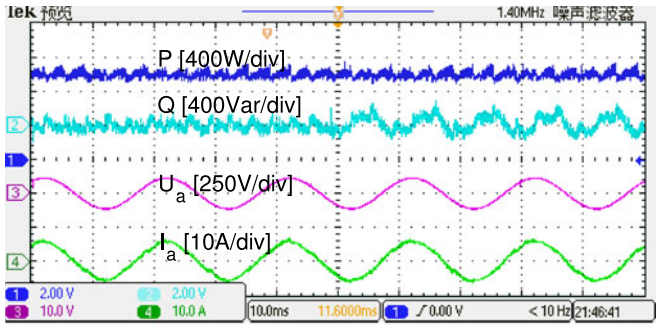

(a)

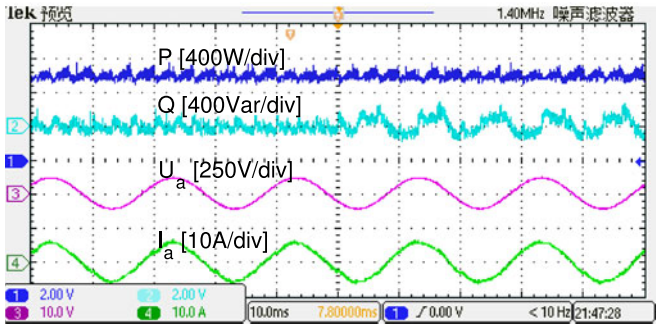

(b)

Fig. 9. Experimental waveform of active power, reactive power, one-phase grid voltage, and one-phase grid current under unbalanced network conditions when changing from the conventional DPC to (a) APOC method I and (b) APOC method II.

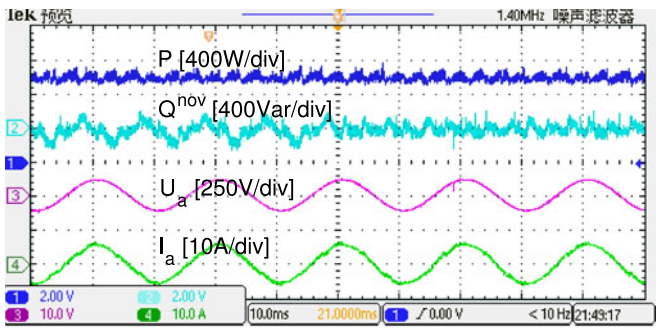

(a)

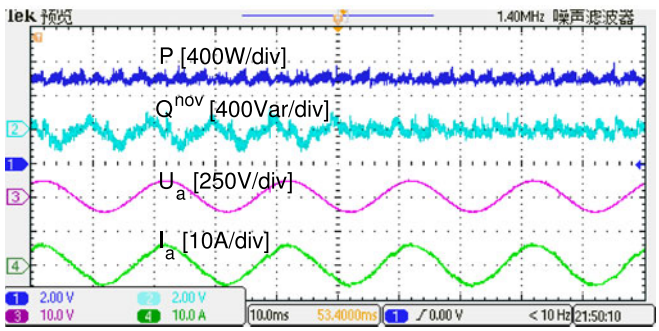

(b)

Fig. 10. Experimental waveform of active power, novel reactive power, one-phase grid voltage, and one-phase grid current under unbalanced network conditions when changing from the conventional DPC to (a) APOC method I and (b) APOC method II ($L = 10$ mH).

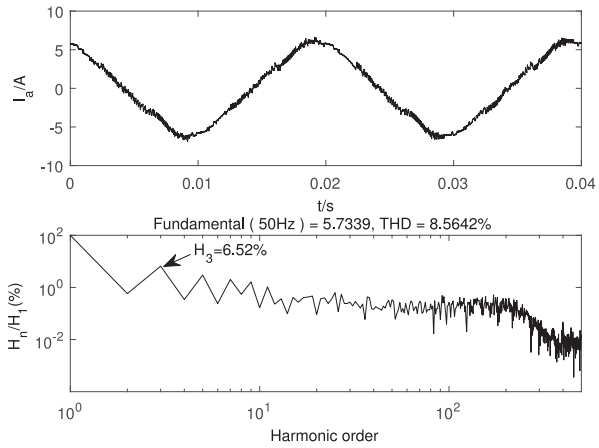

(a)

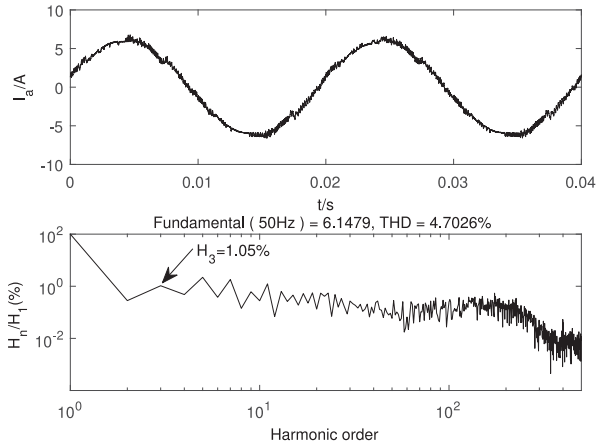

(b)

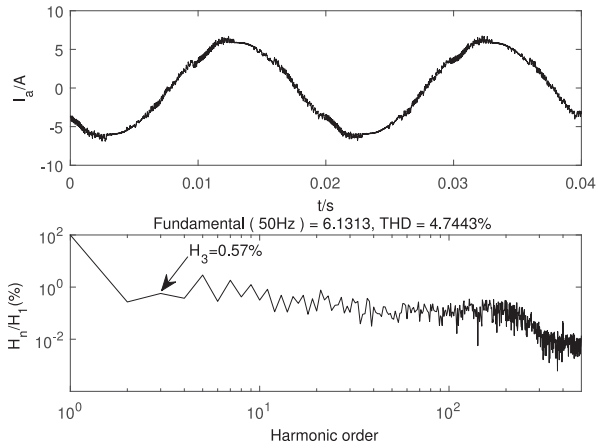

(c)

Fig. 11. Harmonic spectrum of the grid current at $P = 1000$ W and $Q = 0$ Var for (a) conventional DPC, (b) APOC method I, and (c) APOC method II.

B. Dynamic Response

Apart from the steady-state performance comparison of both APOC methods, Fig. 12 further presents the dynamic response to stepped change in the active power reference under unbalanced network, where the active power reference steps from 600 to 1000 W suddenly. It is clearly seen that during the dynamic process, the novel reactive power is constant, and decoupled

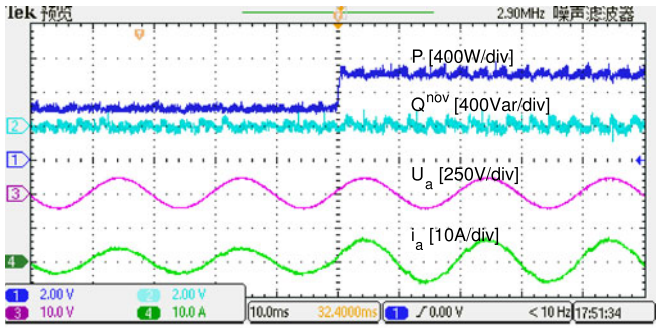

(a)

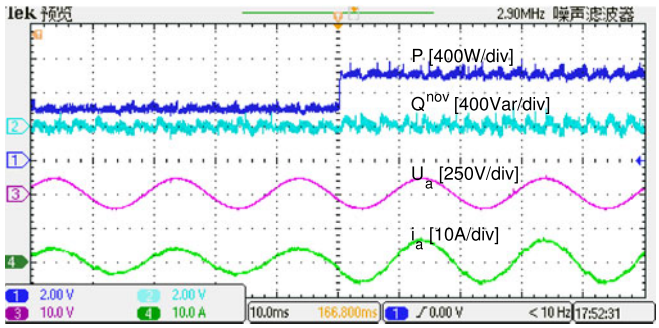

(b)

Fig. 12. Dynamic responses to stepped change in the active power reference under unbalanced network. (a) APOC method I. (b) APOC method II.

control of active power and reactive power is achieved. Both APOC methods I and II achieve very similar dynamic responses to each other. The results confirm their equivalence and effectiveness even in the dynamic process under unbalanced network.

C. Influence of Inductance

According to the principle introduced in Section III, the value of inductance is not used in both APOC methods. Hence, the stability of the proposed APOC method should not be affected by the inductance. Fig. 13 shows the results obtained under the same condition as Fig. 10 except that the inductance is reduced from 10 to 7 mH. It is seen that similar results to Fig. 10 are obtained. As the line inductance is reduced, the power ripples in Fig. 13 are increased compared to Fig. 10. However, the system is still stable and works well under unbalanced network by exhibiting sinusoidal grid current and constant active power and novel reactive power when APOC methods are enabled.

D. DC-Link Voltage Regulation

The above results are obtained under the condition of open-loop dc voltage control, where the power references are directly given. This paper also tests the performance of each method under the condition of closed-loop dc voltage control, where the PI gains are obtained following the principle introduced in [5]. The inductance is reduced from 10 to 7 mH to verify the effectiveness of the proposed APOC methods under unbalanced network. As shown in Fig. 14, the dc-link voltage reference steps from 280 to 320 V. From top to bottom, the curves shown in

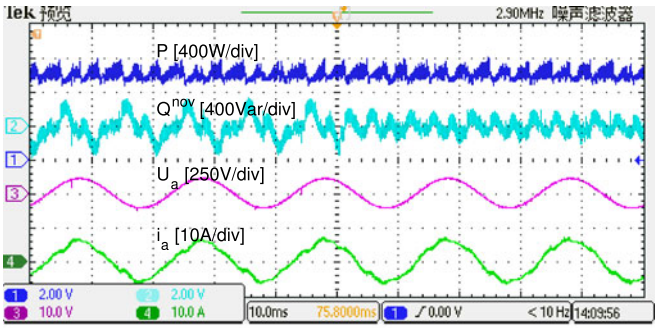

(a)

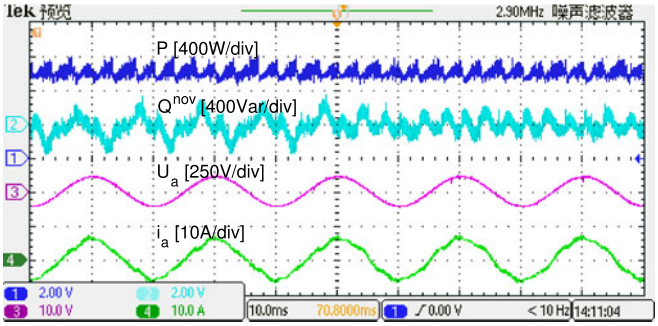

(b)

Fig. 13. Experimental waveform of active power, novel reactive power, one-phase grid voltage, and one-phase grid current under unbalanced network conditions when changing from the conventional DPC to (a) APOC method I and (b) APOC method II ($L = 7$ mH).

Fig. 14 are dc-link voltage, active power, novel reactive power, and one-phase grid current. It is seen that the active power increases linearly with the increase of dc-link voltage. At the same time, the novel reactive power is kept at zero to achieve unity power factor. For conventional DPC, the novel reactive power is oscillating at twice grid frequency and the grid current is highly distorted. On the contrary, the novel reactive power in both APOC methods I and II is constant and the grid current is still sinusoidal in shape, even in the dynamic process of dc-link voltage changes. The results confirm the effectiveness of the proposed APOC methods under unbalanced network and variable dc-link voltage.

E. Comparisons

From all of the experimental results, it is clearly demonstrated that the two APOC methods have similar performance to each other due to their inherent equivalence. However, they have some noticeable difference in principle. The first method is based on conventional power theory and it requires an additional power compensation block. The calculation of power compensation is much simpler than the principle introduced in [24] by eliminating the sequence decomposition of grid voltages and currents. The second method is even simpler than the first method by simply replacing the conventional reactive power with the novel reactive power definition. The control structure remains the same as conventional table-based DPC and it does not require any power compensation technique. Hence, the principle of the second method is much simpler and it is easy to use in practical applications.

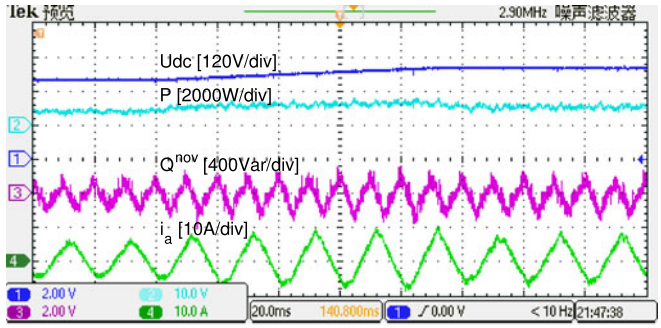

(a)

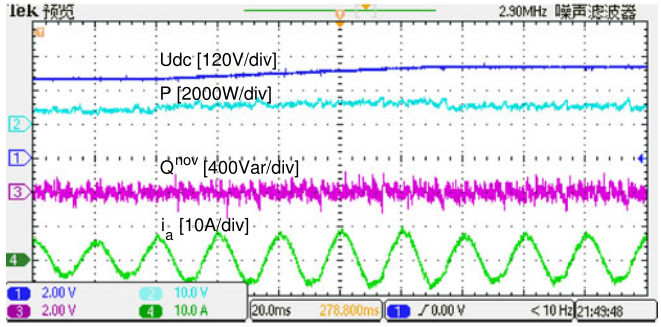

(b)

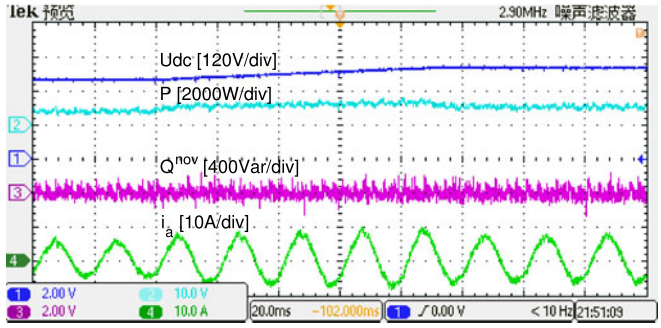

(c)

Fig. 14. Experimental waveform of dc-link voltage, active power, novel reactive power, and one-phase grid current under unbalanced network condition when the dc-link voltage reference steps from 280 to 320 V ($L = 7$ mH). (a) Conventional DPC. (b) APOC method I. (c) APOC method II.

VI. Conclusion

This paper presents two kinds of APOC methods for DPC under the condition of unbalanced network conditions and, what is more, reveals their inherent relationship. Both of them do not require the extraction of positive-/negative-sequence decomposition of grid voltages, rectifier voltages, and grid currents. Hence, they can be easily incorporated into the existing DPC strategies, such as the basic table-based DPC in this paper. The first method modifies the original power references by adding appropriate power compensations. The second one uses the same structure as the basic DPC, except that the reactive power is replaced by a novel reactive power definition. Both methods can achieve constant active power and sinusoidal grid currents, even under the condition of unbalanced grid voltages. Furthermore, it is found that the two methods are inherent equivalent because they produce the same signs of power changes when

selecting the voltage vector from a predefined switching table. The principles of the two methods are explained in detail, and their effectiveness and inherent equivalence are validated by the simulation and experimental results.

REFERENCES

[1] B. Singh, B. N. Singh, A. Chandra, K. Al-Haddad, A. Pandey, and D. P. Kothari, "A review of three-phase improved power quality ac-dc converters," *IEEE Trans. Ind. Electron.*, vol. 51, no. 3, pp. 641–660, Jun. 2004.

[2] Y. Zhang, Z. Li, Y. Zhang, W. Xie, Z. Piao, and C. Hu, "Performance improvement of direct power control of PWM rectifier with simple calculation," *IEEE Trans. Power Electron.*, vol. 28, no. 7, pp. 3428–3437, Jul. 2013.

[3] J. Rodriguez, J. Dixon, J. Espinoza, J. Pontt, and P. Lezana, "PWM regenerative rectifiers: State of the art," *IEEE Trans. Ind. Electron.*, vol. 52, no. 1, pp. 5–22, Feb. 2005.

[4] Y. Zhang and C. Qu, "Direct power control of a pulse width modulation rectifier using space vector modulation under unbalanced grid voltages," *IEEE Trans. Power Electron.*, vol. 30, no. 10, pp. 5892–5901, Oct. 2015.

[5] V. Blasko and V. Kaura, "A new mathematical model and control of a three-phase ac-dc voltage source converter," *IEEE Trans. Power Electron.*, vol. 12, no. 1, pp. 116–123, Jan. 1997.

[6] Y. Zhang and C. Qu, "Table-based direct power control for three-phase ac/dc converters under unbalanced grid voltages," *IEEE Trans. Power Electron.*, vol. 30, no. 12, pp. 7090–7099, Dec. 2015.

[7] T. Noguchi, H. Tomiki, S. Kondo, and I. Takahashi, "Direct power control of PWM converter without power-source voltage sensors," *IEEE Trans. Ind. Appl.*, vol. 34, no. 3, pp. 473–479, May/Jun. 1998.

[8] Y. Zhang, C. Qu, and J. Gao, "Performance improvement of direct power control of PWM rectifier under unbalanced network," *IEEE Trans. Power Electron.*, to be published.

[9] P. Antoniewicz and M. Kazmierkowski, "Virtual-flux-based predictive direct power control of ac/dc converters with online inductance estimation," *IEEE Trans. Ind. Electron.*, vol. 55, no. 12, pp. 4381–4390, Dec. 2008.

[10] P. Cortes, J. Rodriguez, P. Antoniewicz, and M. Kazmierkowski, "Direct power control of an AFE using predictive control," *IEEE Trans. Power Electron.*, vol. 23, no. 5, pp. 2516–2523, Sep. 2008.

[11] Y. Zhang, J. Zhu, Z. Zhao, W. Xu, and D. Dorrell, "An improved direct torque control for three-level inverter-fed induction motor sensorless drive," *IEEE Trans. Power Electron.*, vol. 27, no. 3, pp. 1502–1513, Mar. 2012.

[12] Y. Zhang and H. Yang, "Two-vector-based model predictive torque control without weighting factors for induction motor drives," *IEEE Trans. Power Electron.*, vol. 31, no. 2, pp. 1381–1390, Feb. 2016.

[13] M. Malinowski, M. Jasinski, and M. Kazmierkowski, "Simple direct power control of three-phase PWM rectifier using space-vector modulation (DPC-SVM)," *IEEE Trans. Ind. Electron.*, vol. 51, no. 2, pp. 447–454, Apr. 2004.

[14] Y. Zhang and H. Yang, "Generalized two-vector-based model-predictive torque control of induction motor drives," *IEEE Trans. Power Electron.*, vol. 30, no. 7, pp. 3818–3829, Jul. 2015.

[15] Y. Zhang and H. Yang, "Model predictive torque control of induction motor drives with optimal duty cycle control," *IEEE Trans. Power Electron.*, vol. 29, no. 12, pp. 6593–6603, Dec. 2014.

[16] H. Akagi, Y. Kanazawa, and A. Nabae, "Instantaneous reactive power compensators comprising switching devices without energy storage components," *IEEE Trans. Ind. Appl.*, vol. IA-20, no. 3, pp. 625–630, May 1984.

[17] A. Stankovic and T. Lipo, "A novel control method for input output harmonic elimination of the PWM boost type rectifier under unbalanced operating conditions," *IEEE Trans. Power Electron.*, vol. 16, no. 5, pp. 603–611, Sep. 2001.

[18] P. Rioual, H. Pouliquen, and J.-P. Louis, "Regulation of a PWM rectifier in the unbalanced network state using a generalized model," *IEEE Trans. Power Electron.*, vol. 11, no. 3, pp. 495–502, May 1996.

[19] H.-S. Song and K. Nam, "Dual current control scheme for PWM converter under unbalanced input voltage conditions," *IEEE Trans. Ind. Electron.*, vol. 46, no. 5, pp. 953–959, Oct. 1999.

[20] H.-S. Song, I.-W. Joo, and K. Nam, "Source voltage sensorless estimation scheme for PWM rectifiers under unbalanced conditions," *IEEE Trans. Ind. Electron.*, vol. 50, no. 6, pp. 1238–1245, Dec. 2003.

[21] B. Yin, R. Oruganti, S. K. Panda, and A. K. S. Bhat, "An output-power-control strategy for a three-phase PWM rectifier under unbalanced supply conditions," *IEEE Trans. Ind. Electron.*, vol. 55, no. 5, pp. 2140–2151, May 2008.

[22] J. Eloy-Garcia, S. Arnaltes, and J. Rodriguez-Amenedo, "Direct power control of voltage source inverters with unbalanced grid voltages," *IET Power Electron.*, vol. 1, no. 3, pp. 395–407, 2008.

[23] D. Santos-Martin, J. L. Rodriguez-Amenedo, and S. Arnalte, "Direct power control applied to doubly fed induction generator under unbalanced grid voltage conditions," *IEEE Trans. Power Electron.*, vol. 23, no. 5, pp. 2328–2336, Sep. 2008.

[24] L. Shang, D. Sun, and J. Hu, "Sliding-mode-based direct power control of grid-connected voltage-sourced inverters under unbalanced network conditions," *IET Power Electron.*, vol. 4, no. 5, pp. 570–579, 2011.

[25] Y. Komatsu and T. Kawabata, "A control method of active power filter where system voltage contains negative-phase-sequence component or zero-phase-sequence component," in *Proc. Int. Power Electron. Drive Syst. Conf.*, 1995, pp. 583–586.

[26] Y. Zhang and C. Qu, "Model predictive direct power control of PWM rectifiers under unbalanced network conditions," *IEEE Trans. Ind. Electron.*, vol. 62, no. 7, pp. 4011–4022, Jul. 2015.

[27] Y. Suh and T. A. Lipo, "Modeling and analysis of instantaneous active and reactive power for PWM ac/dc converter under generalized unbalanced network," *IEEE Trans. Power Del.*, vol. 21, no. 3, pp. 1530–1540, Jul. 2006.

[28] Z. Li, Y. Li, P. Wang, H. Zhu, C. Liu, and W. Xu, "Control of three-phase boost-type PWM rectifier in stationary frame under unbalanced input voltage," *IEEE Trans. Power Electron.*, vol. 25, no. 10, pp. 2521–2530, Oct. 2010.

[29] Y. Zhang, C. Qu, Z. Li, and Y. Zhang, "Mechanism analysis and experimental study of table-based direct power control," in *Proc. Int. Conf. Elect. Mach. Syst.*, 2013, pp. 2213–2218.

[30] *IEEE Recommended Practice for Monitoring Electric Power Quality*, IEEE Std 1159-2009 (Revision of IEEE Std 1159-1995), 2009.

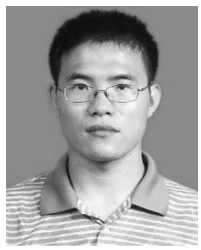

Yongchang Zhang (M'10) received the B.S. degree from Chongqing University, Chongqing, China, in 2004, and the Ph.D. degree from Tsinghua University, Beijing, China, in 2009, both in electrical engineering.

From August 2009 to August 2011, he was a Postdoctoral Fellow with the University of Technology Sydney, Australia. He joined North China University of Technology in August 2011 as an Associate Professor, where he is currently a full Professor and the Vice Director of the Inverter Technologies Engineering Research Center. He has published more than 100 technical papers in the area of motor drives, pulse width modulation, and ac/dc converters. His current research interests include model-predictive control for power converters and motor drives.

Jihao Gao was born in 1988. He received the B.S. degree in electrical engineering from Henan University of Engineering, Zhengzhou, China, in 2013. He is currently working toward the master's degree in electrical engineering from North China University of Technology, Beijing, China.

His research interests include control of three-level pulse width modulation rectifiers.

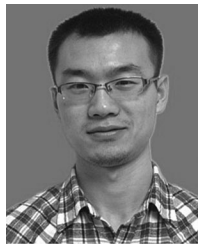

Changqi Qu was born in 1988. He received the B.S. degree from Beijing Jiaotong University, Beijing, China, in 2009, and the master' s degree from North China University of Technology, Beijing, in 2015, both in electrical engineering.

His research interests include control of pulse width modulation rectifiers under unbalanced grid voltages.